Preprint Title	Thiophene/selenophene-based S-shaped double helicenes: regioselective synthesis and structures
Authors	Mengjie Wang, Lanping Dang, Wan Xu, Zhiying Ma, Liuliu Shao, Guangxia Wang, Chunli Li and Hua Wang
Publication Date	27 Apr. 2022
Article Type	Letter
Supporting Information File 1	DH-2.cif; 738.6 KB
Supporting Information File 2	Supporting Information.docx; 10.8 MB
ORCID® iDs	Chunli Li - https://orcid.org/0000-0003-0707-2800

Thiophene/selenophene-based S-shaped double helicenes: regioselective synthesis and structures

Mengjie Wang,‡ Lanping Dang,‡ Wan Xu, Zhiying Ma, Liuliu Shao, Guangxia Wang, Chunli Li * and Hua Wang*

Engineering Research Center for Nanomaterials, Henan University, Kaifeng, 475004, China

Email: chunli79@126.com; hwang@henu.edu.cn

* Corresponding author

‡ Equal contributors

Abstract

2,5-Di(trimethylsilanyl)dithieno[2,3-*b*:3′,2′-*d*]thiophene ((TMS)$_2$-*bb*-**DTT**), 2,5-di(trimethylsilanyl)diseleno[2,3-*b*:3′,2′-*d*]thiophene ((TMS)$_2$-*bb*-**DST**), and 2,5-di(trimethylsilanyl)diseleno[2,3-*b*:3′,2′-*d*] selenophene ((TMS)$_2$-*bb*-**DSS**) were used as starting materials to synthesize three S-shaped double helicenes (i. e., **DH**-**1**, **DH**-**2**, and **DH**-**3**) through monobromination, formylation, the Wittig reaction, and double oxidative photocyclization. Photocyclization was a highly regioselective process. The molecular structures of **DH**-**1** and **DH**-**2** were confirmed by X-ray single-crystal analysis. Multiple intermolecular interactions, such as C-S, C-Se, S-S, S-Se, and Se-Se, were observed in the crystal packing structures of these compounds. Spectroscopic results and our previous work showed that the combination of molecular structure change and heteroatom replacement from S to Se could precisely modulate molecular energy levels.

Keywords

thiophene; selenophene; double helicene; regioselective synthesis; crystal structure

Introduction

Given their esthetically pleasing helical structures, inherent helical chirality, and extended π-conjugation, helicenes have attracted extensive research attention. Helicenes are generally divided into carbohelicenes and heterohelicenes. The rapid development of carbohelicenes has led to the synthesis of double, triple, quadruple, quintuple, and sextuple molecules, the chiro-optical properties of these molecules, such as their circular dichroism (CD) and circularly polarized luminescence (CPL), have also been widely studied [1]. The development of thiahelicene, a class of typical heterohelicenes, has led to the preparation of symmetric thiophene-based [5], [7], [9], and [11]helicenes [2], unsymmetric thiophene-based [7]helicenes [3], and thiophene-based double helicenes with spiro-silicon atoms [4], “saddle” formed 8π annulene [2d], and twisted naphthalene as central spacers [5].

As its close analogue, selenophene has properties very similar to those of thiophene. Fused aromatic compounds containing selenophene units show favorable optical and electrochemical properties and improved charge transport characteristics in the solid state mainly because such fused aromatic compounds often undergo increased Se-Se interactions, which confer ordering at the molecular scale and, thus, lead to well-aligned solid-state packing and excellent charge-transport properties [6].

However, as an important type of heteroacenes, fused selenophenes have rarely been reported in the literature because their synthesis is extremely challenging. The first seven-ring-fused heteroacene containing selenophene was synthesized through the intramolecular triple cyclization of bis(*o*-haloaryl)diacetylene by Yamaguchi in 2005 [7].

Using a similar method, Takimiya reported the synthesis of six-ring-fused and four-ring-fused heteroacenes containing selenopheno[3,2-*b*]selenophene in 2007 and 2009, respectively [8]. Five years later, Cheng reported the synthesis of two types of five-ring-fused isomers of diselenopheno[2,3-*b*:7,6-*b*′]fluorine and diselenopheno[3,2-*b*:6,7-*b*′]fluorene through the cyclization of terminal acetylene as well as six types of biselenophene-based fused tricyclic derivatives [9]. In 2017, we reported the first member of diselenoselenophenes (**DSS**s), 2,5-di(trimethylsilanyl)diseleno[2,3-*b*:3′,2′-*d*]selenophene ((TMS)$_2$-*bb*-**DSS**), the TMS group could easily be removed by trifluoroacetic acid and replaced by bromine [10]. Another isomer of **DSS**, diseleno[3,2-*b*:2′,3′-*d*]selenophene (*tt*-**DSS**) has been successively synthesized from selenophene [11].

Among the limited fused aromatic compounds containing selenophene currently available, helicenes have received relatively little attention [10]. In our previous work, bull horn-shaped selenophene-based heteroacenes (**1**, Figure 1) and selenophene-based [7]helicene (**2**, Figure 1) were synthesized from the (TMS)$_2$-substituted selenophene triacenes, 2,5-di(trimethylsilanyl)diseleno[3,2-*b*:2′,3′-*d*]selenophene ((TMS)$_2$-*tt*-**DSS**) and (TMS)$_2$-*bb*-**DSS**, respectively. In this work, the novel S-shaped double helicene **DH**-**3** (Figure 1), which is based on selenophene units, was constructed as a new member of the selenohelicene family.

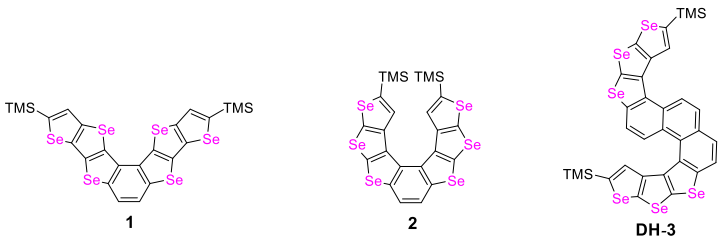

J. Org. Chem., 2018 [11a] *J. Org. Chem.*, 2017 [10] This Work

Figure 1. Molecular structures of **1**, **2** and **DH**-**3**.

In this synthetic study, regioselective double oxidative photocyclization was observed during the construction of three S-shaped double helicenes **DH**-(**1**-**3**) based on thiophene/selenophene. From **DH**-**1** to **DH**-**3**, sulfur atoms in the molecular framework

were gradually replaced by selenium atoms. The crystal structures and spectroscopic features of **DH**-(**1**-**3**) were then studied. Finally, the reaction sites of oxidative photocyclization, energy levels, and the electron cloud distribution of the highest occupied molecular orbitals (HOMOs) and the lowest unoccupied molecular orbitals (LUMOs) are predicted.

Results and Discussion

Synthesis of 5(a-c) and DH-(1-3)

The synthetic route of 1,3-bis(2-(5-(trimethylsilyl)dithieno-[2,3-*b*:3',2'-*d*]thiophen-2-yl)vinyl)benzene (**5a**), 1,3-bis(2-(5-(trimethylsilyl)diselenopheno[2,3-*b*:3',2'-*d*]thiophen-2-yl)vinyl)benzene (**5b**), 1,3-bis(2-(5-(trimethylsilyl)diselenopheno[2,3-*b*:3',2'-*d*] selenophen-2-yl)vinyl)benzene (**5c**), and S-shaped double helicenes **DH-**(**1**-**3**) is shown in Scheme 1. The double oxidative photocyclization of **5**(**a**-**c**) is the key step in the synthesis of **DH**-(**1**-**3**) because oxidative photocyclization induces double radicals on a double bond, which led to the C=C bond rotation along the resulting single C(radical)-C(radical) bond and randomly directed annelated products [12]. Moreover, **5a**-**c**, bear two C=C bonds, which may lead to more complex photocyclization products. 5-Trimethylsilanyl-diseleno[2,3-*b*:3′,2′-*d*]thiophene-2-carbald-ehyde (**4a**), 5-trimethylsilanyl-diseleno[2,3-*b*:3′,2′-*d*]thiophene-2-carbaldehyde (**4b**) and 5-trimethylsilanyl-diseleno[2,3-*b*:3′,2′-*d*]selenophene-2-carbaldehyde (**4c**) were prepared via monobromination and formylation reactions with $(TMS)_2$-*bb*-**DTT**, $(TMS)_2$-*bb*-**DST**, and $(TMS)_2$-*bb*-**DSS** as starting materials according to the literature [10]. After the double Wittig reaction of **4**(**a**-**c**) and 1,3-phenyldimethyltriphenylphosphoniumbromide **5a** and **5b** were synthesized with yields of 46% and 64%, respectively. After the double Wittig reaction of **5c** we obtained a mixture of *cis* and

trans isomers with the total yield of 50%. According to the results of ^{1}H NMR the ratio of *cis* and *trans* isomers was approximately 1:0.25.

Compound **5** had five isomers and three reaction sites (2, 4, and 6-positions in the benzene moiety) during oxidative photocyclization. Irradiation of **5**(**a**-**c**) resulted in oxidative photocyclization products with two types of configurations wherein two benzene rings were closed in the same and opposite direction, such as **DH**-(**1**-**3**) and **6** (Figure 2). However, after the double oxidative photocyclizations of **5**(**a**-**c**) in the presence of iodine and propylene oxide in dry toluene through irradiation by a 450 W Hg medium-pressure lamp for 1.5 h, only one type of ring-closing product with two benzene rings formed in the same direction, i. e., S-shaped double helicenes **DH**-(**1**-**3**) are obtained in yields of 62%, 30%, and 53%, respectively.

The double oxidative photocyclization reaction sites of **5** were predicted by the orbital-weighted Fukui function in Multiwfn using Gaussian 09 [13] at the B3LYP/6-31G**[14] level of theory to verify the reaction-site selectivity of oxidative photocyclization further. Results showed that the conformations of **5a** are varied, but orbital-weighted Fukui function has nothing to do with conformation. In the orbital-weighted Fukui function, the larger the isosurface distribution, the higher the activity of free radical reactions. Thus the 4- and6-positions of benzene are the most likely sites for the free radical reaction (Figure S20). However, after the formation of the naphthalene ring, the α position is the most likely site for free radical reaction (Figure S21). Therefore, after the double oxidative photocyclization of compound **5a**, **DH**-**1** is mainly obtained. The predicted result of the double oxidative photocyclizations of **5a** is consistent with the experimental result, that is, an S-shaped double helicene can be selectively obtained through the double oxidative photocyclization of compound **5a**.

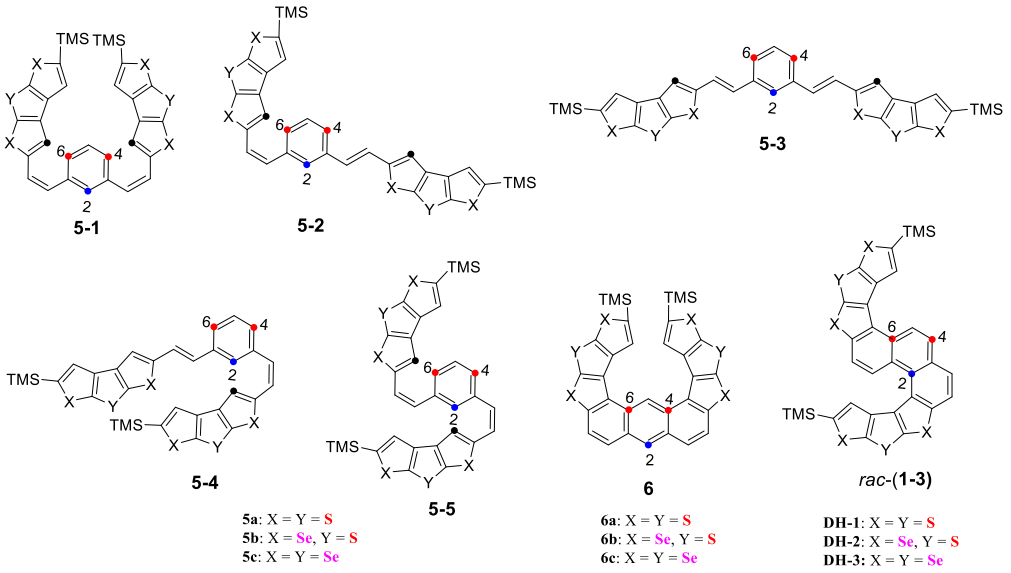

Figure 2. Five kinds of isomer structures of **5** and two kinds of possible oxidative photocyclization product structures of **6** and **DH**-(**1**-**3**).

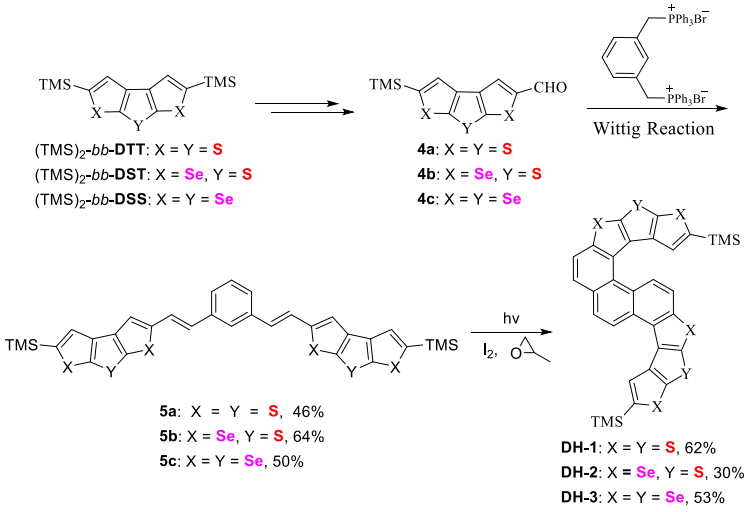

Scheme 1. Synthetic route to S-shaped double helicenes **DH**-(**1**-**3**).

Crystallographic analyses of DH-1 and DH-2

The molecular structures of **DH**-**1** and **DH**-**2** were confirmed by single-crystal analysis (Figure 3). Both **DH**-**1** and **DH**-**2** belong to the triclinic space group P-1. After double oxidative photocyclizations of **5a** and **5b**, **DH**-**1** and **DH**-**2** are compressed into S-shaped double helical structures (Figures 3A, 3B), which consist of one [5]helicene and one [6]helicene. The two helicenes have the same configuration and bend toward the same direction on the same side of the shared naphthalene ring (Figures 3C, 3D).

Both **DH**-**1** or **DH**-**2** feature a pair of enantiomers *MM* and *PP* in the unit cell (Figures S24, 28). The crystal parameters of **DH**-**1** and **DH**-**2** are shown in Table 1.

Table 1. Crystal parameters of **DH**-**1** and **DH**-**2**

Compounds		Dihedral angles (°)[a]	Torsions Angles (°)[b]	Turn angles in- plane (°)[c]	Helix climbs (Å)[d]
DH-1	[5]helicene	25.00	38.64	231.1	0.932
	[6]helicene	50.61	64.38	273.6	2.424
DH-2	[5]helicene	25.01	37.27	230.9	0.879
	[6]helicene	48.16	64.12	279.3	2.462

[a]Dihedral angle between two terminal rings of helicene. [b]The sum of the three ([5]helicene) or four ([6]helicene) distortion angles. [c]The angle of turns in-plane. [d]Internal helix climb height.

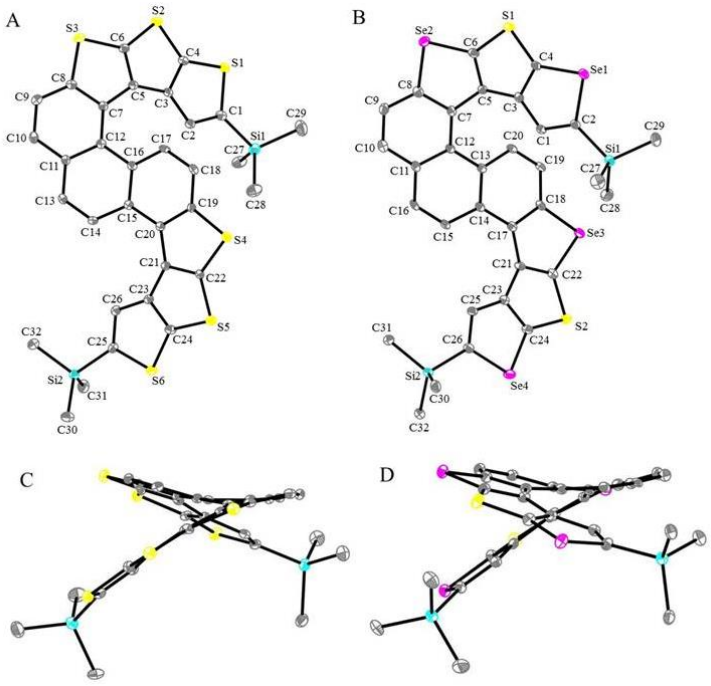

Figure 3. Molecular structures and side view for **DH**-**1** and **DH**-**2.** A and B are molecular structures for **DH**-**1** and **DH**-**2**. C and D are side view for **DH**-**1** and **DH**-**2**. Carbon, sulfur, selenium, and silicon atoms are depicted with thermal ellipsoids set at the 30% probability level, and all hydrogen atoms are omitted for clarity.

Each of the two **DH**-**1** molecules (blue and red molecules, Figure S25) in the unit cell interacts with six adjacent molecules. For example, in Figure S25, the blue molecule interacts with six adjacent molecules through multiple interactions, such as, S···S (3.44

Å), S···H (2.94 Å, 2.91 Å, 2.97 Å), H···H (2.31 Å), C···C (3.31 Å), S···C (3.45 Å), and C···H (2.90 Å). Each of the two **DH**-**2** molecules (blue and red molecules, Figure S29) in the unit cell interact with eight adjacent molecules. For example, in Figure S29, the blue molecule interacts with eight adjacent molecules through multiple interactions, such as, C···C (3.40 Å), Se···H (3.09 Å), H···H (2.26 Å), C···H (2.90 Å), Se···Se (3.62 Å), and Se···S (3.58 Å). However, in contrast to **DH**-**1**, **DH**-**2** exhibits multiple S···H (2.88 Å), S···C (3.45 Å), and Se···H (2.94 Å) interactions between two molecules in the unit cell. These multiple interactions confer **DH**-**1** and **DH**-**2** with a regular arrangement featuring multi channels (Figures S26, 30), which is a suitable characteristic for helicene compounds used as supramolecular self-assembly units [15].

Spectroscopic Features of DH-(1-3)

The UV-vis absorption spectra of **DH**-(**1**-**3**) in dichloromethane are shown in Figure 4. The UV-vis absorption spectra of **DH**-(**1**-**3**) are generally similar in shape and exhibit three major absorption bands within 230-280 nm (Band-I), 280-330 nm (Band-II), and 304-414 nm (Band-III) (Figure 4). Progressive red-shifts in the absorption spectra of Band-I, Band-II, and Band-III occur with increasing number of selenium atoms. In Band-I, compounds **DH**-(**1**-**3**) show a maximum absorption peak at 232, 240, and 242 nm, respectively. In Band-II and Band-III, helical distortion and possible conjugation through heteroatoms (e. g., sulfur and selenium atoms) in **DH**-(**1**-**3**) may increase π-electron delocalization, which causes the molecules to show red-shifted broad absorption. The maximum absorption peaks of **DH**-(**1**-**3**) occur at 268, 275, 279 nm, respectively, in Band-II and 323, 331 and 336 nm, respectively, in Band-III. Thus, the optical band gaps estimated from the absorption edges gradually decrease from **DH**-**1** to **DH**-**2** to **DH**-**3**, and are equal to 3.08, 3.01, and 2.98 eV, respectively. This change

trend is consistent with the calculated results, which are 3.97, 3.83, and 3.81 eV for **DH**-**1**, **DH**-**2**, and **DH**-**3**, respectively (Table S2). However, the optical band gaps of **1**, **2**, and **DH**-**3** obviously differ because of changes in their molecular configuration and equal to 2.86, 3.15, and 3.81 eV, respectively [10, 11a]. As the number of selenium atoms increases from **DH**-**1** to **DH**-**3**, the fluorescence intensity (Figure S18) and fluorescence quantum yield (Φ_F, Figure S19, and Table S1) of the molecules also decrease.

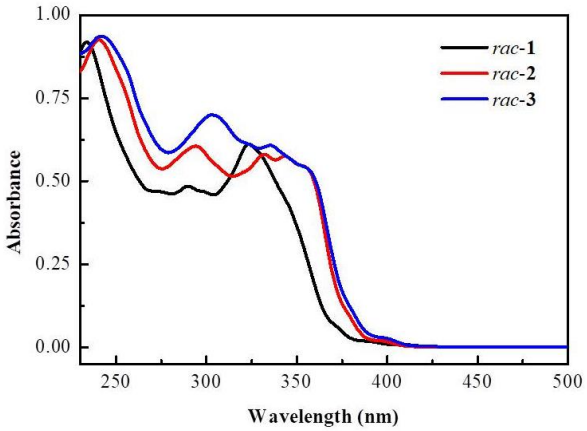

Fig. 4. UV-vis absorption spectra of **DH**-(**1**-**3**) in CH_2Cl_2 ([C] = 1×10^{-5} M).

Conclusion

In summary, the key step of regioselective double oxidative photocyclization was successfully employed in the preparation of three S-shaped double helicenes, namely, **DH**-**1**, **DH**-**2** and **DH**-**3** with $(TMS)_2$-*bb*-**DTT**, $(TMS)_2$-*bb*-**DST**, and $(TMS)_2$-*bb*-**DSS** as starting materials. The synthetic method described in this research not only provides a method for the synthesis of S- shaped double helicenes but also enriches the family of selenophene helicenes. Multiple intermolecular interactions and regular arrangement in the crystal packing structures of **DH**-**1** and **DH**-**2** indicate that these compounds may be used as supramolecular self-assembly units. Changes in molecular structure may substantially modulate the optical band gap of heteroacenes, and the replacement of

heteroatoms from S to Se could fine-tune their optical band gap [4, 10, 11a]. Thus, the combination of molecular structure modification and atom replacement could be a viable strategy, for the precise modulation molecular energy levels and yield molecules with strong application potential in organic functional materials, such as OFETs, and CPLs, among others.

Experimental

General Procedures and Materials

Tetrahydrofuran (THF) for use on vacuum line were freshly distilled from sodium/benzophenone prior to use. *n*-BuLi (hexane) were obtained from Energy Chemical; prior to use, its concentration was determined by titration with *N*-pivaloyl-*o*-toluidine [16]. Column chromatography was carried out on silica gel (300-400 mesh). Analytical thin-layer chromatography was performed on glass plates of silica gel GF-254 with detection by UV. Standard techniques for synthesis under inert atmosphere and Schlenk glassware equipped with an 8 mm PTFE vacuum stopcock, were employed. All starting materials and reagents were commercially available.

^{1}H NMR and $^{13}C\{^{1}H\}$ NMR spectra were recorded on 300 or 400 MHz NMR instrument using $CDCl_3$ as solvents. The chemical shift references were as follows: (^{1}H) $CDCl_3$, 7.26 ppm ($CHCl_3$); ($^{13}C\{^{1}H\}$) $CDCl_3$, 77.00 ppm ($CDCl_3$). IR spectra were obtained using an FT-IR instrument. MS analysis was carried out on mass spectrometers equipped with EI (70 eV). HRMS analysis was carried out on a mass spectrometer equipped with DART-FT-ICR and MALDI-TOF-CHCA. Melting-point determination was taken on a Melt-Temp apparatus and was uncorrected. The X-ray crystallographic analyses were performed using crystals of compounds **DH-1** and **DH-2** with sizes of 0.14 × 0.12 × 0.08, 0.21 × 0.17 × 0.12 mm^3, respectively. The intensity data were

collected with the *ω* scan mode (296 K) on a diffractometer with CCD detector using Cu Kα radiation (λ = 1.54184 Å). The data were corrected for Lorentz and polarization effects, and absorption corrections were performed using SADABS program [17]. The crystal structures were solved using the SHELXTL program and refined using full-matrix least-squares [18]. Further details are in the deposited CIF files. Slow evaporation of solutions of **DH**-**1** and **DH**-**2** in $CHCl_3$-CH_3OH (5:1 v/v) were employed for growing single crystals. The fluorescence quantum yields (Φ_F) of **DH**-(**1**-**3**) are characterized in dichloromethane with quinine sulfate in 0.1 N H_2SO_4 as the control.

Synthesis of 5(a-c) and DH-(1-3)

Synthesis of 1,3-bis(2-(5-(trimethylsilyl)dithieno[2,3-b:3',2'-d]thiophen-2-yl)vinyl)-benzene (5a)

n-BuLi (0.06 mL, 2.50 M in hexane, 0.168 mmol, 2.5 eq) was added dropwise to 1,3-bis[methyl(bromotriphenylphosphonium)] (53.3 mg, 0.067 mmol) in THF (40 mL) at -78 °C. After 2 h at -78 °C, the solution of **4a** (41.0 mg, 0.138 mmol, 2.05 eq) in THF (5 mL) was added at -78 °C and kept for 1 h, and then the reaction mixture was warmed up slowly to ambient temperature overnight. The reaction mixture was quenched with CH_3OH and extracted with CH_2Cl_2 (3 × 10 mL). The organic layer was washed with saturated NaCl (20 mL) and water (2 × 20 mL), and then dried over $MgSO_4$. The residue was purified by column chromatography (eluent: HEX/CH_2Cl_2 (v/v = 3/1)) and recrystallization from $CHCl_3$-CH_3OH to yield **5a** (20.9 mg, 46%) as a yellow solid, mp: > 300 ^oC. ^1H NMR (400 MHz, $CDCl_3$), *δ* (ppm): 7.58 (s, 1H), 7.45 (s, 2H), 7.41-7.36 (m, 3H), 7.34 (s, 2H), 7.31 (d, *J* = 16.0 Hz, 2H), 6.93 (d, *J* = 16.0 Hz, 2H), 0.39 (s, 18H). $^{13}C\{^1H\}$ NMR (100 MHz, $CDCl_3$), *δ* (ppm): 145.3, 144.7, 143.7, 140.7, 138.4, 137.8, 137.2, 129.1, 127.8, 125.5, 124.9, 124.4, 122.8, 118.0, -0.1. MS (EI, 70 eV): m/z =

662.18 (40) $[M]^+$. HRMS (MALDI) m/z $[M]^+$ calcd for $C_{32}H_{30}S_6Si_2$ 662.0216; found 662.0205. IR (KBr): 3018, 2958, 2849, 1631, 1408, 1360, 945, 837 cm^{-1}.

1,3-bis(2-(5-(trimethylsilyl)diselenopheno[2,3-*b*:3',2'-*d*]thiophen-2-yl)vinyl)benzene (**5b**) was synthesized according to the compound **5a** procedure. **5b**: yellow solid in yield of 64% (46.2 mg), mp: > 300 ^oC. ^1H NMR (300 MHz, $CDCl_3$), δ (ppm): 7.73 (s, 2H), 7.55 (d, *J* = 15.0 Hz, 3H), 7.38-7.32 (m, 5 H), 6.79 (d, *J* = 15.0 Hz, 2H), 0.38 (s, 18H). $^{13}C\{^1H\}$ NMR (100 MHz, $CDCl_3$), δ (ppm):151.6, 149.7, 144.5, 142.6, 141.1, 137.01, 136.98, 129.2, 128.6, 127.5, 125.6, 124.9, 124.4, 121.0, 0.2. MS (DART): m/z = 854.8 (75) $[M + H]^+$. HRMS (DART) m/z $[M + H]^+$ calcd for $C_{32}H_{31}S_2Se_4Si_2$ 854.8071; found 854.8067. IR (KBr): 3011, 2949, 2891, 1627, 1427, 1367, 920, 831 cm^{-1}.

1,3-bis(2-(5-(trimethylsilyl)diselenopheno[2,3-*b*:3',2'-*d*]selenophen-2-yl)vinyl)benzene (**5c**) was synthesized according to the compound **5a** procedure. mixture of cis and trans isomers **5c**: yellow solid in yield of 50% (24.4 mg), mp: > 300 ^oC. ^1H NMR (400 MHz, $CDCl_3$), δ (ppm): 7.76 (s, *trans*-), 7.73 (s, *cis*- and *trans*-), 7.72 (s, *cis*- and *trans*-), 7.57 (s, *cis*- and *trans*-), 7.56 (s, *trans*-), 7.49-7.33 (m, *trans*-, *cis*- and *trans*-), 7.30 (d, *J* = 16.0 Hz, *cis*- and *trans*-), 6.90 (d, *J* = 12.0 Hz, *cis*- and *trans*-), 6.79 (d, *J* = 16.0 Hz, *trans*-), 6.78 (d, *J* = 16.0 Hz, *trans*- and *trans*-), 6.65 (d, *J* = 12.0 Hz, *cis*- and *trans*-), 0.38 (s, *trans*-), 0.36 (s, *cis*- and *trans*-), 0.35 (s, *cis*- and *trans*-). The ratio of integral areas of the peaks at 7.76, 7.73 and 7.72 ppm is 1.0 : 0.25. MS (MALDI): m/z = 949.8 $[M^+]$. HRMS (DART-FT) m/z $[M]^+$ calcd for $C_{32}H_{30}Se_6Si_2$ 949.6894; found 949.6887. IR (KBr): 3010, 2951, 2889, 1624, 1413, 1369, 908, 833 cm^{-1}.

Synthesis of DH-1

To a solution of **5a** (9.6 mg, 0.014 mmol) in dry toluene (6 mL), iodine (7.3 mg, 0.028 mmol, 2.0 eq) and excess propylene oxide was added. The reaction solution was irradiated with a 450 W unfiltered Hg medium-pressure lamp for 1.5 h. The reaction

was quenched with saturated $Na_2S_3O_3$ (5 mL). The reaction mixture was extracted with CH_2Cl_2 (3 × 5 mL), washed with H_2O (3 × 10 mL), and then dried over $MgSO_4$. After removing the solvent in vacuum, the crude product was purified by PTLC with petrol ether (60-90 °C) HEX/CH_2Cl_2 (v/v = 5/1) as developer to yield **DH**-**1** (5.9 mg, 62%) as a light-yellow solid, mp: >300 °C. ^{1}H NMR (400 MHz, $CDCl_3$), δ (ppm): 9.09 (d, J = 12.0 Hz, 1H), 8.51 (d, J = 8.0 Hz, 1H), 8.22 (s, 1H), 8.11 (d, J = 8.0 Hz, 1H), 8.04 (d, J = 8.0 Hz, 1H), 7.90 (d, J = 8.0 Hz, 1H), 7.78 (d, J = 8.0 Hz, 1H), 6.62 (s, 1H), 0.48 (s, 9H), 0.14 (s, 9H). ^{13}C{^{1}H} NMR (100 MHz, $CDCl_3$), δ (ppm): 144.6, 144.1, 143.19, 143.18, 142.1, 141.7, 141.6, 141.4, 141.3, 141.1, 135.0, 133.4, 130.6, 129.8, 129.0, 128.5, 127.53, 127.46, 127.3, 127.0, 126.7, 126.4, 124.3, 123.7, 121.5, 119. 7, 0.0, -0.4. MS (EI, 70 eV): m/z = 657.87 (30) $[M]^+$. HRMS (MALDI) m/z $[M]^+$ calcd for $C_{32}H_{26}S_6Si_2$ 657.9896; found 657.9892. IR (KBr): 3045, 2952, 2860, 1645, 1487, 1410, 972, 837 cm^{-1}.

DH-**2** was synthesized according to the compound **DH**-**1** procedure. **DH**-**2**: light-yellow solid in yield of 30% (15.8 mg), mp: >300 °C. ^{1}H NMR (400 MHz, $CDCl_3$), δ (ppm): 8.92 (d, J = 8.0 Hz, 1H), 8.54 (s, 1H), 8.32 (d, J = 8.0 Hz, 1H), 8.04 (d, J = 8.0 Hz, 1H), 7.95 (d, J = 8.0 Hz, 1H), 7.80 (d, J = 8.0 Hz, 1H), 7.66 (d, J = 8.0 Hz, 1H), 6.66 (s, 1H), 0.47 (s, 9H), -0.01 (s, 9H). ^{13}C{^{1}H} NMR (100 MHz, $CDCl_3$), δ (ppm): 149.9, 146.9, 145.7, 145.1, 144.8, 144.3, 142.7, 142.6, 139.8, 139.4, 139.2, 137.5, 132.8, 130.8, 130.6, 130.2, 129.59, 129.58, 128.4, 128.1, 126.7, 125.6, 124.5, 124.3, 124.2, 122.2, 0.3, -0.2. MS (DART): m/z = 850.8 (45) $[M + H]^+$. HRMS (DART) m/z $[M + H]^+$ calcd for $C_{32}H_{27}S_2Si_2Se_4$ 850.7758; found 850.7743. IR (KBr): 3060, 2949, 2896, 1632, 1489, 1402, 933, 829 cm^{-1}.

DH-**3** was synthesized according to the compound **DH**-**1** procedure. **DH**-**3**: light yellow solid in yield of 53% (19.5 mg), mp: 265.1-266.9 ^{o}C. ^{1}H NMR (300 MHz, $CDCl_3$), δ (ppm): 8.86 (d, J = 9.0 Hz, 1H), 8.56 (s, 1H), 8.22 (d, J = 9.0 Hz, 1H), 8.06 (d, J = 9.0

Hz, 1H), 7.92 (d, *J* = 9.0 Hz, 1H), 7.82 (d, *J* = 9.0 Hz, 1H), 7.64 (d, *J* = 9.0 Hz, 1H), 6.68 (s, 1H), 0.45 (s, 9H), -0.11 (s, 9H). $^{13}C\{^{1}H\}$ NMR (150 MHz, $CDCl_3$), δ (ppm): 151.0, 148.0, 147.4, 147.0, 145.9, 143.9, 142.6, 141.1, 140.9, 139.34, 139.26, 138.9, 134.1, 132.3, 131.7, 130.7, 130.2, 129.3, 128.8, 128.0, 126.7, 125.0, 124.9, 124.1, 123.9, 121.9, 0.4, -0.3. MS (DART): m/z = 945.8 $[M]^+$. HRMS (DART-FT) m/z $[M]^+$ calcd for $C_{32}H_{26}Se_6Si_2$ 945.6580; found 945.6564. IR (KBr): 3047, 2947, 2895, 1633, 1504, 1409, 925, 831 cm^{-1}.

Supporting Information

Supporting Information File 1:

NMR and HRMS spectra, fluorescence spectra, and computational data, crystallographic CIF files of **DH**-**1** and **DH**-**2** (CCDC 2125978 and 2125979).

Acknowledgements

This research was financially supported by the NSFC (U2004213, 21672054) and The Key Technologies R&D Program of Henan Province (212102210627).

References

1. Mori, T. *Chem. Rev.*, **2021**, *121*, 2373-2412.

2. (a) Miyasaka, M.; Rajca, A. **Synlett**, **2004**, 177-181. (b) Zhang, C.; Ma, Z.; Wang, G.; Li, C.; Wang, H. *Org. Chem. Front.* **2020**, *7*, 3926-3934. (c) Rajca, A.; Wang, H.; Pink, M.; Rajca, S. *Angew. Chem. Int. Ed.* **2000**, *39*, 4481-4483. (d) Li, C.; Shi, J.; Xu, L.; Wang, Y.; Cheng, Y.; Wang, H. *J. Org. Chem.* **2009,** *74*, 408-411. (e) Liu, X.; Sun, H.; Xu, W.; Wan, S.; Shi, J.; Li, C.; Wang, H. *Org. Chem. Front.* **2018**, *5*, 1257-1261. (f) Rajca, A.; Miyasaka, M.; Pink, M.; Wang, H.; Rajca, S. *J. Am. Chem. Soc.*

2004, *126*, 15211-15222. (g) Miyasaka, M.; Pink, M.; Olankitwanit, A.; Rajca, S.; Rajca, A. *Org. Lett.* **2012**, *14*, 3076-3079. (i) Miyasaka, M.; Rajca, A.; Pink, M.; Rajca, S. *J. Am. Chem. Soc.* **2005**, *127*, 13806-13807.

3. Wang, J.; Wang, G.; Li, C.; Dong, Y.; Ma, Z.; Wang, H. *J. Org. Chem.* **2021**, *86*, 4413-4422.
4. Li, C.; Wu, L.; Xu, W.; Song, J.; Shi, J.; Yu, P.; Kan, Y.; Wang, H. *J. Org. Chem.* **2015**, *80*, 11156-11161.
5. Wang, Z.; Shi, J.; Wang, J.; Li, C.; Tian, X.; Cheng, Y.; Wang, H. *Org. Lett.* **2010**, *12*, 456-459.
6. (a) Hollinger, J.; Gao, D.; D. Seferos, S. *Isr. J. Chem.* **2014**, *54*, 440-453. (b) Patra, A.; Bendikov, M. *J. Mater. Chem.* **2010**, *20*, 422-433.
7. Okamoto, T.; Kudoh, K.; Wakamiya, A.; Yamaguchi, S. *Org. Lett.* **2005**, *7*, 5301-5304.
8. (a) Yamamoto, T.; Takimiya, K. *J. Am. Chem. Soc.* **2007**, *129*, 2224-2225. (b) Izawa, T.; Miyazaki, E.; Takimiya, K. *Chem. Mater.* **2009**, *21*, 903-912.
9. (a) Pao, Y.-C.; Chen, Y.-L.; Chen, Y.-T.; Cheng, S.-W.; Lai, Y.-Y.; Huang, W.-C.; Cheng, Y.-J. *Org. Lett.* **2014**, *16*, 5724-5727. (b) Lee, C.-H.; Lai, Y.-Y.; Cheng, S.-W.; Cheng, Y.-J. *Org. Lett.* **2014**,*16*, 936-939.
10. Xu, W.; Wu, L.; Fang, M.; Ma, Z.; Shan, Z.; Li, C.; Wang, H. *J. Org. Chem.* **2017**, *82*, 11192-11197.
11. (a) Xu, W.; Wang, M.; Ma, Z.; Shan, Z.; Li, C.; Wang, H. *J. Org. Chem.* **2018**, *83*, 12154-12163. (b) Schwartz, P.-O.; Förtsch, S.; Vogt, A.; Mena-Osteritz, E.; Bäuerle, P. *Beilstein J. Org. Chem.* **2019**,*15*, 1379-1393.
12. Liu, X.; Yu, P.; Xu, L.; Yang, J.; Shi, J.; Wang, Z.; Cheng, Y.; Wang, H. *J. Org. Chem.* **2013**, *78*, 6316-6321.

13. (a) Pino-Rios, R.; Yañez, O.; Inostroza, D.; Ruiz, L.; Cardenas, C.; Fuentealba, P.; Tiznado, W. *Journal of Computational Chemistry* **2017**, *38*, 481-488. (b) Fu, R.; Lu, T.; Chen, F.-W. *Acta Phys.-Chim. Sin.* **2014**, *30*, 628-639.

14. Frisch, M. J.; Trucks, G. W.; Schlegel, H. B.; Scuseria, G. E.; Robb, M. A.; Cheeseman, J. R.; Scalmani, G.; Barone, V.; Mennucci, B.; G. Petersson, A.; Nakatsuji, H.; Caricato, M.; Li, X.; Hratchian, H. P.; Izmaylov, A. F.; Bloino, J.; Zheng, G.; Sonnenberg, J. L.; Hada, M.; Ehara, M.; Toyota, K.; Fukuda, R.; Hasegawa, J.; Ishida, M.; Nakajima, T.; Honda, Y.; Kitao, O.; Nakai, H.; Vreven, T.; Montgomery, J. A.; Peralta, J. E.; Ogliaro, F.; Bearpark, M.; Heyd, J. J.; Brothers, E.; Kudin, K. N.; Staroverov, V. N.; Kobayashi, R.; Normand, J.; Raghavachari, K.; Rendell, A.; Burant, J. C.; Iyengar, S. S.; Tomasi, J.; Cossi, M.; Rega, N.; Millam, J. M.; Klene, M.; Knox, J. E.; Cross, J. B.; Bakken, V.; Adamo, C.; Jaramillo, J.; Gomperts, R.; Stratmann, R. E.; Yazyev, O.; Austin, A. J.; Cammi, R.; Pomelli, C.; Ochterski, J. W.; Martin, R. L.; Morokuma, K.; Zakrzewski, V. G.; Voth, G. A.; Salvador, P.; Dannenberg, J. J.; Dapprich, S.; Daniels, A. D.; Farkas, O.; Foresman, J. B.; Ortiz, J. V.; ioslowski, C J.; Fox, D.; gaussian, J. *Inc., Wallingford CT* **2013**.

15. (a) Ernst, K. H.; Bohringer, M.; McFadden, C. F.; Hug, P.; Muller, U.; Ellerbeck, U. *Nanotechnology* **1999**, *10*, 355-361. (b) Taniguchi, M.; Nakagawa, H.; Yamagishi, A.; Yamada, K. *Surf Sci.* **2000**, *454*, 1005-1009. (c) Taniguchi, M.; Nakagawa, H.; Yamagishi, A.; Yamada, K. *J. Mol. Catal. Chem.* **2003**, *199*, 65-71. (d) Fasel, R.; Parschau, M.; Ernst, K. H. *Angew Chem. Int. Ed.* **2003**, *42*, 5178-5181. (e) Fasel, R.; Parschau, M.; Ernst, K. H. *Nature* **2006**, *439*, 449-452. (f) Lovinger, A. J.; Nuckolls, C.; Katz, T. J. *J. Am. Chem. Soc.* **1998**,*120*, 264-268. (g) Li, P.; Lai, Y.; Wang, Y.; Qian, Y.; Duan, W.; Li, C.; Wang, Z.; Fang, Q.; Wang, H.; Tu, B.; Geng,

Y.; Zeng, Q. *Sci China Chem.* **2018**, *61*, 844-849. (h) Zhang, G.; Tan, J.; Zhou, L.; Liu, C.; Liu, J.; Zou, Y.; Narita, A.; Hu, Y. *Org. Lett.* **2021**, *23*, 6183-6188.

16. Pieken, W. A.; Kozarich, J. W. *J. Org. Chem.* **1989**, *54*, 510-512.
17. Sheldrick, G. M. *SADABS*, University of Gottingen: Germany, **1996**.
18. Sheldrick, G. M. *SHELXTL*, version 5.1; Bruker Analytical Xray Systems, Inc.: Madison, WI, **1997**.